RADAR IMAGING OF THE PLANETS USING THE VERY LARGE ARRAY

DUANE O. MUHLEMAN and BRYAN J. BUTLER
California Institute of Technology
MARTIN A. SLADE
Jet Propulsion Laboratory
and
ARIE W. GROSSMAN
University of Maryland

1. Introduction

We have used the VLA to make images of the planets which are continuously illuminated by the high power planetary radar transmitter on the 70 meter antenna at Goldstone, CA. That instrument is capable of transmitting up to 460,000 watts of continuous power near 8.5 GHz. Radar imaging experiments became possible after the installation of the 8.5 GHz receivers on all VLA antennas by NASA for the encounter of the Voyager spacecraft with Uranus. A similar radar may be configured with the Australia Telescope (array) at Narrabri and the Goldstone 70 m at S-band which may be important for experiments on Venus whose atmosphere strongly absorbs at X-band. Highly successful experiments have been carried out at the VLA on Mercury, Venus, Mars, Saturn's rings and Titan, the giant satellite of Saturn.

The precise frequency of the transmitter is controlled by a programed local oscillator such that the doppler shift due to the relative motion of the planet's center of mass with respect to the transmitter and the phase center of the VLA is removed and the VLA sees a fixed-frequency signal, except for frequency broadening caused by the rotation of the planet. The CW transmitted signal is spread in frequency due to the variations in the line-of-sight velocities of the reflection points caused by the rotation of the planet relative to the Earth. In the limit of a perfectly spherical planet, the echo power in a frequency interval of f to f+df is created by the reflections from a (doppler) strip parallel to the instantaneous, apparent rotation vector projected on the sky. The total frequency width of the spread spectrum is proportional to the component of the apparent planetary spin vector perpendicular to the radar line of sight and the planet radius. Obviously, there is no radar signal outside that band and the maximum sensitivity is achieved by observing with a bandwidth that matches the radar doppler spectrum. Thus, all experiments have been done in the VLA Spectral Line mode. The echo signal is treated like any natural spectral line source and the full compliment of the VLA software can be used in the signal and image processing.

The transmitted signals are either pure right circular polarized (RCP) or left circular polarized (LCP). The reflected signal at the VLA can be received in both RCP and LCP but with restrictions on the frequency resolution. If a planet is a perfectly smooth, complex dielectric, homogenous sphere, all of the reflected energy

J.G. Robertson and W.J. Tango (eds.), Very High Angular Resolution Imaging, 457–468.

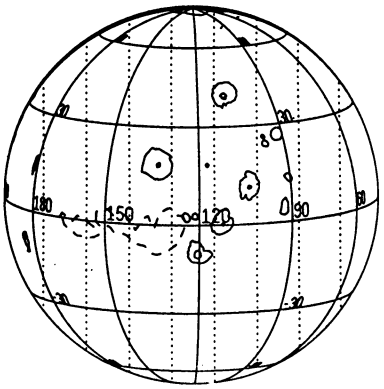

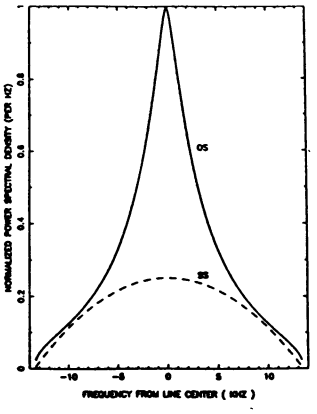

Fig. 1.

(a) A globe of Mars as seen from the Earth on Dec. 8, 1992 shows the bands of constant radar doppler shift for resolution of 3.052 kHz

(b) synthetic Mars radar spectra in circular polarization in opposite sense to that transmitted (OS) and the same sense (SS) as transmitted

is be returned in the Opposite Sense (OS) circular polarization. A natural, inhomogeneous and generally rough planetary surface will return power in all polarizations for RCP or LCP illumination (see below), i.e., both OS and the Same Sense (SS) circular polarization, and the crossed modes.

2. Observing Strategies

The total doppler spreads at X-band vary somewhat with the exact celestial geometry but are about: 400 Hz (Mercury), 100 Hz (Venus), 27,000 Hz (Mars) and 1,350 Hz (Titan). The doppler spreads of the Galilean satellites range from about 1000 Hz to 8000 Hz. The hardware and software of the VLA put strict limits on the choices of frequency resolution and received polarization. The MINIMUM frequency resolution at the VLA is (at least currently) 381 Hz and only a SINGLE circular polarization can be recorded in that mode (Single IF mode). The minimum resolution for which both RCP and LCP can be recorded is 763 Hz. THe minimum resolution in which all 4 Stokes parameters can be recovered is 1526 Hz. Thus, polarization experiments on Mercury, Venus and Titan are seriously compromised, i.e., channel bandwidths wider than the radar signals must be employed, significantly reducing the sensitivity of the experiments by a factor of the square root of the ratio of the total doppler spread to the channel resolution. The circumstances are illustrated for Mars in Figure 1a which shows the geometry of the planet at an epoch on December 29, 1992 when the martian central meridian longitude of the subearth point was 122 deg. Several major martian structures are sketched on the figure including the three 28 kilometer high volcanoes on the Tharsis Ridge eastward of 120 deg. and Olympus Mons at 130 degrees. The dotted lines illustrate the doppler strips with channel separations of 3.052 KHz. A model of the average doppler spectra observed from Mars in OS and SS polarization are shown

https://doi.org/10.1017/S0074180900108186 Published online by Cambridge University Press

in Figure 1b (with infinite frequency resolution). An actual Mars spectrum would display anomalous power in the doppler strips containing Olympus Mons, etc. along with all the power averaged over the surface corresponding to the given strip. The important differences between the OS and SS responses will be discussed below. The "doppler mapping" technique has long been done with monostatic planetary radars where north/south resolution is poorly determined with numerical inversion techniques. The great advance with the VLA/Goldstone radar is primarily the unambiguous spatial imaging of the reflected power and secondarily, an increase in collecting area over the 70 m operated as a monostatic radar. An additional advantage with the VLA is the continuous operation allowed by the separation of the transmitter from the receiver. Clearly, Mars could be observed with resolution of 24.4 KHz (which would exclude the echoes from the east and west equatorial limbs) or 48.8 KHz which would accept a noise bandwidth twice that of the signal. Our observing strategy for Mars is to make 15 minute snapshots because of the rapid planetary rotation and to observe with channel spacing of 3.05 KHz which is a little larger than the rotational smearing during the snapshot. Each channel map is calibrated and separately cleaned, then recombined into snapshot images. The advantages of this technique are discussed in the next section. Observations of Venus, Mercury and, to some extent, Titan are seriously compromised by frequency resolution limits at the VLA!

An additional limitation of the VLA hardware and software results from the necessarily narrow total bandwidth of the continuum "channel". Simultaneous mapping of the thermal emission from the planet's surface would be extremely complimentary to the radar imaging because both emission and reflection are primarily controlled by the physics of the surface/space interface. In most cases the reflectivity and emissivity are compliments; they are not necessarily so where diffuse or multiple scattering are important, which includes several important near surface structures. Currently, it is not possible to simultaneously record a broadband continuum channel for thermal emission and narrowband spectral line channels for the radar at the VLA.

3. Coherent, Pseudo–Coherent, and Incoherent Reflections

The reflection of an electromagnetic wave at a dielectric interface (such as a planetary surface) can be generally understood as a solution of Maxwell's equations with the proper boundary conditions. However, the rigorous solution of this problem for boundary conditions which are only statistically described remains a major unsolved problem of classical physics! Born approximation solutions exist for highly restricted problems involving small surface undulations relative to the wavelength, small slopes, and no shadowing. Even these approximate solutions are restricted to surfaces with gaussianly distributed height variations and gaussian correlation functions. The actual variations on planetary surfaces in the presence of gravity and erosion tend to be exponential. A moderately successful description of the problem which is far from rigorous was presented by Muhleman (1964). He assumed that the radar echo from a real planet is primarily controlled by the angle and size distributions of "flat facets" on the surface which act like mirrors undergoing Fresnel

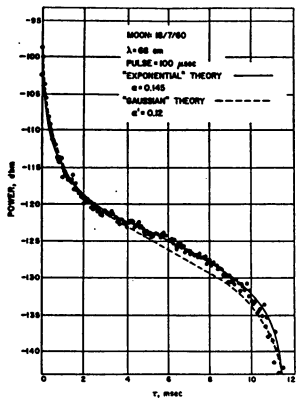

Fig. 2. Measurements of the lunar backscattering function at wavelength of 68 cm and theoretical scattering models. The time delay is measured from the subradar point on the planet and is proportional to the cosine of the incidence angle.

reflection. They only reflect significant power back to the radar if they are aligned close to perpendicular to the radar line of sight. While such a model is remarkably accurate in representing polarized or OS echoes from the Moon and terrestrial planets, it is incapable of explaining diffuse reflections, depolarization and volume scattering and radiative transfer in the near surface since these phenomena require a true full wave treatment including diffraction effects. Such a development is not in sight although detailed Monte Carlo simulations on very large computers will become important in the near future.

Using exponentially distributed surface height variations and Poisson distribution of scale sizes, Muhleman(1964) obtained the following expression for the OS backscattered power as a function of incidence angle x

$$P(x) = \left(\frac{a}{\sin(x) + a \cos(x)} \right)^3 \tag{1}$$

which has been normalized to unity at normal incidence, $x = 0$. Examples of the success of the flat facet theory are shown in the next 2 figures. Narrow pulse observations of the Moon are shown in Figure 2 as a function of time delay, $\tau = 11.6 \cos(x)$ (msec), the relationship between depth from the front point of a sphere to the annulus at incidence angle x. The dashed line in the figure shows the scattering function for gaussian and rayleigh height and length scale distributions. The exponential function fits the entire sphere with a single parameter, a, which is proportional to a mean rms, one - dimensional slope of the surface roughness. Data taken 40 years later on Mercury with the VLA/Goldstone radar are shown in Figure 3. In this case, VLA images were made of the entire planet for OS (polarized) polarization on the right and SS (depolarized) polarization on the left (Butler,et al.,1993). The data points were generated by annulus averaging the images from the subearth point to the limb of Mercury. The remarkable enhancements right at the pole in both polarizations is the signature of polar ice and will be discussed below. The fit of equation (1) to the OS image is shown by the solid line in the right panel and

https://doi.org/10.1017/S0074180900108186 Published online by Cambridge University Press

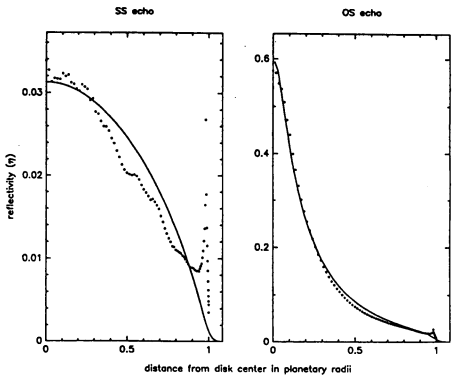

Fig. 3. Measured scattering laws for Mercury and scattering models. Data are annulus averages of the VLA radar images.

a simple $\cos(x)$ scattering model is shown for the SS image. Similar results for OS measurements of Venus and Mars are also explained to this precision with the flat facet model.

We note in passing that side-looking radars and synthetic aperture radars (SAR's) flown on spacecraft and aircraft for radar imaging of the Earth and Venus use the equivalent to OS imaging but usually with parallel linear polarization. Thus, these images are dominated by surface slope distributions (relative to the radar line of sight) and weakly sense subsurface effects such as multiple scattering and the effects of absorption, i.e., the measurements are relatively insensitive to the surface composition.

Given the success of the flat facet model, even though it is far from rigorous, we can consider it as a model for interferometric imaging of planetary surfaces. Such a facet would display a diffraction scattering function at a wavelength ω and size s given by

$$S(x) \sim \left(\frac{\sin(y)}{y}\right)^2 \tag{2}$$

where $y = 6.28(sx/\omega)$. The width of the main lobe of the scattering function is approximately ω/s radians. The reflection from a single facet can be thought of as *coherent* and the facet will contribute a coherent reflection during the interval when the radar line-of-sight is within this main lobe. At any instant of time, when an entire planet's surface is illuminated with a monochromatic plane wave, the model suggests that an uncountable number of facets will be aligned with the radar line-of-sight in their major diffraction lobes. Most of the contributing facets will be near the subradar point but they will occur all the way to the limb where they would have vertical slopes. Because in all cases the planet is rotating relative the the radar, the contributing facets will continually change with time depending on their size and the wavelength, w. We have no real idea what the facet size, s, actually is for any planet including the Earth! The Earth has never been observed with a radar illuminating most of the globe at great distance. We can crudely bound s with the

https://doi.org/10.1017/S0074180900108186 Published online by Cambridge University Press

following arguments. The facet must be flat with respect to a wavelength in order to produce a coherent reflection (which is required to make the flat facet or geometrical optics model work). It is difficult to imagine any geological or geochemical process that would produce structures flat with respect to our wavelength of 3.5 cm larger than about 50 m. Furthermore, the facets (that count) must be larger than our wavelength or they produce diffuse scattering. Therefore, we adopt 1 meter as the minimum size of the facets. Now we can consider the behavior of the individual planets within these limits. At any instant of time, the signal presented to the VLA is the sum of all the point sources which are individually coherent. However, this sum is incoherent since each point source is at a different distance from the wave front. (The point source signals are at slightly different frequencies due to the differential doppler shifts caused by the rotation of the planet but that effect is very small). We estimate a "coherence time" or a time interval in which the ensemble of point sources as seen by the VLA is "fixed". These values are shown in the following table:

Planet	Sidereal Period	Coherence Time 1 meter facets	Coherence Time 50 meter facets
Moon	27 days	3.6 hours	260 sec
Mercury	57 days	7.6 hours	550 sec
Venus	243 days	32.4 hours	39 min
Mars	1.02 days	8.4 min	10 sec

We can see from the table that the OS image is roughly fixed to order 10 hours if the facets are strongly distributed near 1 m sizes but the coherence time is of order of minutes if they are much larger. For Mars, the OS image completely changes in less than 10 minutes. Thus, the VLA calibration procedures must consider each case separately. We consider the calibration techniques next.

4. Calibration of VLA Radar Images

At any instant of time, the radar signals to the VLA are the same as that from any natural spectral line source. However, the actual signal varies with time; rapidly for Mars but slowly for the other planetary objects. The amplitude and phase of the instrument are calibrated as a function of time by generating complex gain tables from 1 or 2 standard VLA point source calibrators (QSO's). In addition, we use the quasi-specular "spike" from the center of the planet contained in the OS IF for a phase-only selfcalibration for both IF's. That is, the central part of the OS spectrum illustrated in Figure 1 is used as a selfcalibration beacon. In each case, only the central radar channel is used for selfcalibration which for Mercury and Venus (and the Moon in the future) is the only channel in the radar spectrum. We have carried out this procedure using equation (1) as the source model (which is very time consuming) and in a second method, by just using a few CLEAN components which is much faster but considerably less accurate. The results are similar but we

are still evaluating both procedures. This technique does not properly selfcalibrate the receiver phase errors in the SS IF but removes phase fluctuations caused by the atmosphere , the signal reference system and antenna position errors. It greatly improves both the SS and OS images.

Images of Mars are made at about 15 minute intervals since we are looking at a different section of the planet for each snapshot. Titan and Saturn's rings are a special case since neither object has a quasi-specular component in the OS IF. This occurs because both are essentially cold ice which is highly transparent at X-band and the "coherent" true surface reflections are unimportant. Radar images of Saturn's rings are the same for OS and SS polarization. That is probably true for Titan but signals from that source are so near the sensitivity limit of the VLA/Goldstone radar selfcalibration with this technique is not possible. Additionally, the thermal emission from the disk of Saturn is always in the Titan images. A uniform disk model of Saturn is used to generate the selfcalibrated gain tables for the Titan experiments.

5. Planetary Results

All of the planetary objects considered about have been extensively investigated since the 1960's using the standard monostatic mapping technique. Ranging modulation is used on a phase coherent transmitted signal which allows one to both spectrally and temporally sort the echo data to create intersecting doppler strips and range rings. The technique has serious technical difficulties for rapidly rotation planets such as Mars and is even a problem for Mercury. Recent work at Arecibo by John Harmon and others has allowed them to overcome some of the difficulties. In all cases, however, the doppler-range-gated maps have a north/south ambiguity which can not be completely eliminated. Essentially all of the monostatic work on the planets until recently was limited to studies near the instantaneous subearth point on the target. Clearly, VLA imaging suffers from none of these difficulties and a complete image of the entire Earth-facing hemisphere can be made in a few minutes for nearby planets at a spatial resolution of about 150 km. Our most difficult and perhaps most interesting target is Titan which we must treat nearly as a point source because of its minimum distance of 9 AU. We will review the more interesting VLA scientific results for Mars, Mercury and Titan in this section.

5.1. Mars

We observed Mars on Oct 22, 1988 when it was near opposition (0.46 AU) and the VLA was in the A-array, the largest configuration. This circumstance did not repeat until January, 1993 and we are in an observing program as this is being written. Preliminary results for the first observations appear in Muhleman, et al.1991. Snapshot images were made at about 15 minute intervals, 38 in all. A subset of 6 images at hourly intervals is shown Figure 4. These images are in the SS polarization, free from the quasi-specular spike, and revealed rich new details about Mars. The martian latitude of the Earth was -24 deg. and we were presented with an excellent view of the south pole.The pole turns out to be the strongest radar feature on the

https://doi.org/10.1017/S0074180900108186 Published online by Cambridge University Press

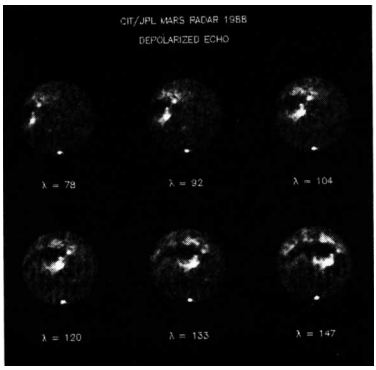

Fig. 4. Six snapshot radar images of Mars made in Oct. 1988 at the VLA. Each snapshot was averaged over 15 minutes and they are an hour apart. The central meridian longitude is indicated for each image. Maps are in SS polarization.

entire planet even though we were viewing it at an incidence angle 66 deg. The echo came from the the Residual South Polar Ice Cap which is slightly off the true pole and remains visible throughout the martian year after the seasonal CO_2 frost has sublimated away. The measured reflectivity of the ice cap is nearly unity which is very similar to the icy surfaces of Europa and Ganymede. Ice at temperatures below 150 K is highly transparent at centimeter wavelengths with an absorption length of 10's of meters and a small real dielectric constant of 3 in its most dense state. The very large reflectivity is interpreted to mean that the ice is highly fractured and the enhanced reflectivity arises from nearly conservative multiple scattering. An additional surprise is that this ice has not lost the fractures by annealing at Mars' temperatures. One of the major goals of our 1993 Mars campaign is to address these questions about the north polar ice sheet (which is warmer on average). Unfortunately, if the scattering process is multiple, conservative scattering we can only place a weak limit on the thickness of the ice layer at thicker than 2 to 5 meters. New observations at longer wavelengths would help greatly.

Another unique feature of Mars can be seen in Figure 4, the black band just north of the equator which is nearly 2000 km in length. We have named this feature "Stealth" since we detected no echo power from it in either polarization. An outline of the structure is indicated by the dashed lines in Figure 1. The interpretation of Muhleman, et al.,1991 is that it is a deposit of highly underdense, ash- like material which probably was blown down the slope of the Tharsis Ridge which is the east limit of Stealth. The deposit must be deeper than several meters or we would see a reflection from the subsurface. Our viewing angle to Stealth in 1988 were never less than 20 off the normal which makes our radar models of the feature rather ambiguous. We will cross Stealth at normal incidence during the 1993 campaign which will allow us to remove some of the ambiguity.

Addition radar observations at longer wavelengths would be of considerable additional help in understanding Stealth and the ice deposits. S-band observations between Goldstone and the Australia Telescope may be feasible. The other bright

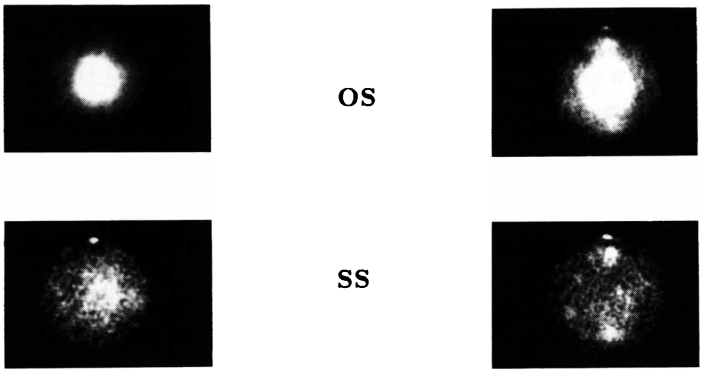

Fig. 5. VLA radar images of Mercury made on Aug. 8 (left) and Aug. 23 (right). The north polar feature appears at the top.

radar features are all associated with the Tharsis volcanoes and Olympus Mons, probably related to relatively young lava flows. We will not discuss them further here. Interestingly, essentially all the radar features were found in unexpected places and forms. The radar images are an unique data source since they are dominated by subsurface effects. Our current knowledge of Mars is high "superficial".

5.2. Mercury

We observed Mercury when it was near an inferior conjunction and the VLA was in the A-array on August 8 and August 23 in 1991. The planet rotated about 100 deg. during that period. The four images obtained are shown in Figure 5 with the Aug.8 view on the left, OS images above and SS images below. The OS images are dominated by the quasi-specular spike but the brightest feature after that is on the Mercury north pole in all four images! Furthermore, the north pole pixels are brighter in depolarization (SS) than in the so-called polarized (OS) mode. This is similar to the returns from the Galilean icy satellites and probably is characteristic of multiple scattering in a relatively transparent medium. The same effect can be seen in Figure 3 which shows the enhanced brightness for the annulus average near the limb even though the north pole contribution has been greatly averaged down with all the other limb pixels. Preliminary results appear in Butler, et al.,1993 and in Slade, et al., 1992. Shortly after our discovery of the north polar feature, it was confirmed at Arecibo by Harmon and Slade, 1992. Harmon also reanalyzed earlier Arecibo observations and was able to show that a very similar feature resides on the Mercury south pole. The existence of a bright feature on both poles argues strongly that the scattering medium is a temperature dependent volatile, which when coupled with its polarization properties strongly suggests ice (Butler,et al,1993).

Detailed calculations of the stability of water ice in the Mercury environment are presented in Butler,et al.,1993. Our observations in 1991 were made when the Mercury-Earth geometry allowed us to look down on the north pole at a grazing angle of about 11 deg. Persuasive arguments can be made that the spin axis of

Mercury is exactly perpendicular to its orbit. Thus, Mercury has zero obliquity, the Sun is always on its equator. Even so, Mercury is sufficiently close to the Sun that a limb of the Sun always illuminates a smooth Mercury surface at the pole. However, the ice safely resides in the permanently shadowed craters and cracks within about 100 km of the poles. Ice and water in general is only safe where it is trapped in polar craters. Water would exist as ice on the surface at night but would evaporate at sunrise and bounce around the surface until it hits a night spot again where it is safe until the next sunrise, hits a permanently shadowed spot where it is safe forever, or is lost forever by dissociation by solar photons. Thus, the poles are cold fingers for the water vapor (and other volatiles such as carbon dioxide and ammonia). The sources of the water include planetary outgassing and water brought to Mercury by meteorites and comets.

Further investigations of the ice deposits is extremely important since they must contain the history of the origin of the inner solar system in their chemical trace elements! An important new motivation has been found to mount a spacecraft mission to Mercury.

5.3. Titan

Titan is one of the most interesting objects in the solar system. It has a dense, cold atmosphere of primarily molecular nitrogen at a surface pressure and temperature of about 1.5 bars and 95 K. The temperature falls along an adiabat to an altitude of about 50 km at a temperature of 70 K, staying just above the liquid temperature of nitrogen. Above that lies a relatively warm stratosphere ($\sim$ 200 K) containing a great array of hydrocarbons and nitriles which rain or snow out below the cold trap. Methane exits throughout the atmosphere at about the 2% level. It was believed that the reservoir for the methane was a global ocean of liquid ethane and methane, perhaps as deep as kilometers. We have showed with the VLA/Goldstone radar that this global ocean does not exist but the puzzling variation in the reflectivity that we measure as Titan rotates under the subradar point could be caused by ethane/methane lakes. Liquid hydrocarbons deeper than a hundred meters would greatly depress the X-band reflectivity to about 2% while our average measured value is 30%. The latter is consistent with a dirty ice surface such as Callisto's.

The disk of Titan at closest approach is 0.8 arc sec in diameter. While we can slightly resolve it at the VLA in the B array and resolve it rather well in the A array, the signal/noise is insufficient for such measurements to be useful considering the strict limitations at the Goldstone 70 meter and the VLA. The total reflected radar power expressed as a flux density varies between 15 and 40 millijanskys. The VLA sensitivity at 3.5 cm in the required narrowband of 381 Hz is about +/- 7 mJ. in the 4 hours integration time available from the joint visibility from the two observatories, and the loss of 2.5 hours for the round trip propagation time. There is a loss of time because the transmitter is nearly an hour west of the VLA. We primarily use the VLA for its collecting area but the ability to measure visibility phase is very important for the detection proposes. Titan is always within about 1 arc minute of Saturn which is a strong thermal emission source and creates confusion problems which in some geometries adds more nonrandom beam noise greater than

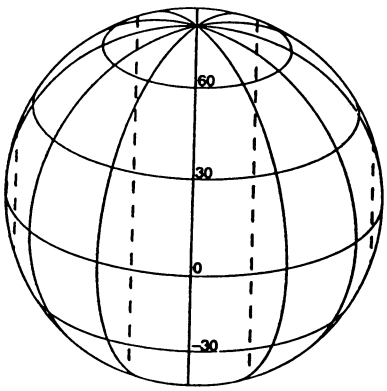

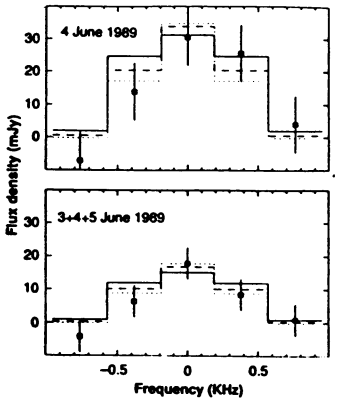

Fig. 6.
(a) Narrowest possible VLA doppler strips (381 Hz) on the geometry of Titan in June, 1989.
(b) Measured Titan radar spectra plotted over the spectra from cosine scattering laws.

the system noise of 7 mJ.

The essential results of our first Titan experiment in June, 1989 are illustrated in Figure 6 which shows the doppler strips at the smallest possible VLA resolution of 381 Hz in the top panel and the observed radar spectra below (see Muhleman,et al., 1990). Since only 1 polarization can be used with the narrow channel width, we only measured the OS polarization. The reflectivity was determined to be 0.35+/-0.08 relative to an equivalent conducting sphere. No ethane ocean. Figure 6b shows that the spectrum is nearly that of a diffuse cosine scattering law all the way to the limbs without a quasi-specular spike. That is consistent with a rough surface and is similar to that seen on the icy satellites of Jupiter.

We show the radar spectra for experiments during the last four years, all in the OS polarization in Figure 7. However, after the first experiment we sacrificed our ability to resolve the disk with doppler strips in order to measure spectra in both polarizations, i.e., we used a channel spacing of 763 Hz. Only on three days out of 11 did we detect a believable SS spectrum and on 2 of those days it was as strong as any OS spectra that we have measured. A strong depolarized echo is the signature of multiple scattering in a transparent medium, e.g.,ice on Mars, Mercury, the Galilean satellites. We don't understand why the phenomenon comes and goes on Titan. We are apparently seeing a considerable variation in the near surface structure over the satellite.

Titan is not only unique because of its atmosphere but it also has an eccentric orbit with an eccentricity of 0.029. That value calls into question the assumption that the rotation of Titan is synchronous with its orbit around Saturn. An extreme example of this is the 2/3 spin resonance of Mercury with respect to its orbital period around the Sun caused by the large eccentricity of its orbit. It is at least possible that the otherwise inexplicable variations of reflectivity and polarization that we observe from day to day and from year to year could be understood if the rotation is nonsynchronous. The orbital period of Titan is 15.945 days. If the

https://doi.org/10.1017/S0074180900108186 Published online by Cambridge University Press

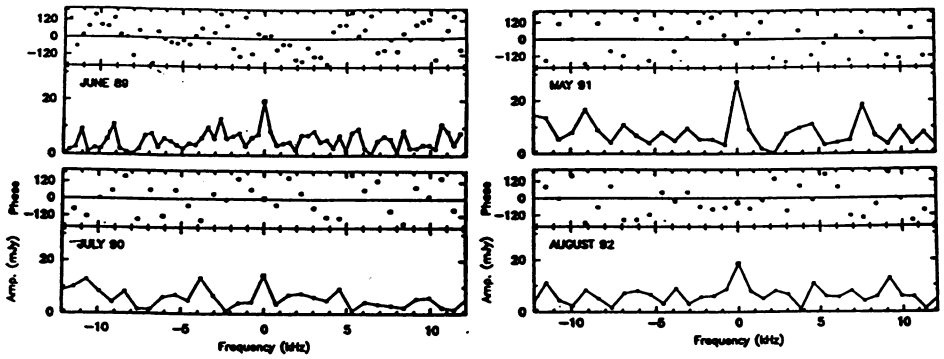

Fig. 7. Titan VLA radar, complex spectra for 3 or 4 day periods at the closest approach of the Saturn system to the Earth during the summers of 1989 through 1992. The phase of the averaged visibility is shown in the upper part of each panel and the amplitude in the lower part. Radar reflection energy can only appear in the center channel of each plot. The remaining channels contain the 3.5 cm thermal emission from Titan, plus noise. Note that the phase of the radar channel is near zero in each case. It is expected to be uniformly distributed in all other channels since the thermal emission is smaller than the system noise in the relevant bandwidth of 763 Hz.

rotational period is about 0.8 HOURS shorter than synchronous, our variations from year to year tend to line up on the new Titan longitude grid. This degree of nonsynchronous rotation would arise if Titan is too weak to support even a small permanent bulge. However, our measurements are so close to the sensitivity limit of the instrument that many more measurements are required to answer these important questions.

The observations are becoming more favorable as the declination of the Saturn system moves north. It is still at - 17 deg and will reach the equator in a few years. When it is a northern source it will be possible to make resolved images of Titan in the B array and possibly after some technical improvements, in the A array. Questions of the rotational rate and direction, variations of surface compositions, the existence of mountain ranges (of ice?), etc. will remain vital for Planetary Science!

References

Butler, B.J., D.O. Muhleman and M.A. Slade: 1993, 'Mercury: Full Disk Radar Images, and the Detection and Stability of Ice at the North Pole', In press, *J. Geophys. Res.*

Harmon, J.K. and M.A. Slade: 1992, 'Radar Mapping of Mercury: Full–Disk Delay–Doppler Images', *Science* **258**, 640–643

Muhleman, D.O., B.J. Butler, A.W. Grossman and M.A. Slade: 1991, 'Radar Images of Mars', *Science* **253**, 1508–1513

Muhleman, D.O., A.W. Grossman, B.J. Butler and M.A. Slade: 1990, 'Radar Reflectivity of Titan', *Science* **248**, 975–980

Muhleman, D.O.: 1964, 'Radar Scattering from Venus and the Moon', *Astron. J.* **69**, 34–41

Slade, M.A., B.J. Butler and D.O. Muhleman: 1992, 'Mercury Radar Imaging: Evidence for Polar Ice', *Science* **248**, 635–640